HTD-Vol. 329, National Heat Transfer Conference
Volume 7
ASME 1996

THERMAL AND HYDRAULIC ANALYSIS OF A HIGH FLUX HEAT EXCHANGER

Mike Cutbirth and Afshin J. Ghajar
School of Mechanical and Aerospace Engineering
Oklahoma State University
Stillwater, Oklahoma 74078

ABSTRACT

With new navigation and high powered radar equipment requiring numerous data processing units, today's military aircraft is experiencing an increase in dependence on electronics. Furthermore, modern technology is constantly creating electronic chips that are capable of more power without increasing the surface area, thereby causing larger heat fluxes. Due to the combination of these factors, new techniques need to be developed for the heat removal of the electronic components. One such technique is the High Flux Heat Exchanger, HFHE, developed by McDonnell Douglas. The HFHE consists of 20 Compact High Intensity Coolers, CHICs, developed by Sundstrand and capable of handling 100 W/cm^2, each with a footprint of one square centimeter, arranged in parallel in one Navy Standard Electronic Module, SEM-E. This translates to a total cooling capacity of 2000 W. The design point for this HFHE is to deliver the 2000 total Watts of cooling capacity while maintaining a junction temperature of less that 90°C and using the synthetic oil polyalphaolefin (PAO) as the coolant.

The concern of this paper is to summarize the analysis of the performance, both hydraulically and thermally, of the HFHE throughout the steady state operation of the electronic components. Because the HFHE contains 20 CHICs in *parallel*, each CHIC performs independently. Therefore, the heat transfer tests can be performed for one CHIC at a time. The tests matrix was constructed by varying the flow rate though the HFHE from 60 to 240 kg/hr by an increment of 15 kg/hr; the coolant temperature of the PAO entering the HFHE from -10 to 40°C by an increment of 10°C; and the heat load applied from 0 to 100 W by an increment of 20 W. Using these results allows for the estimation of the parameters needed for the electronic coolant system using the HFHE. These parameters include the pump size and flow rate needed for sufficient thermal performance of the HFHE.

NOMENCLATURE

A	cross-sectional area of the individual channels of the CHIC, m^2
C	constant relating the Reynolds number and the friction factor for laminar flow
C_n	constants in the curve fit for the pressure, with n =1,2
D	diameter of the individual channels in the CHIC, m
f	friction factor for pipe flow, dimensionless
g	gravitational acceleration, m^2/s
g_c	gravitational constant, kg·m/N·s^2
h_f	total frictional head loss, m
k	thermal conductivity of the HFHE (copper), 300 W/m·°C
k_i	minor loss coefficient for the CHIC for pipe flow, dimensionless
L	length of the individual tubes in the CHICs, m
$\dot{m}$	mass flow rate of the fluid, kg/hr
p	pressure, psi
Re	Reynolds number (= ρVD/μ), dimensionless
R	thermal resistance, °C/(W/cm^2)
r_n	distance from CHIC center to symmetry boundary in n-direction, m
Q	volumetric flow rate, m^3/hr
$\dot{Q}$	heat transfer, W/cm^2 or W per CHIC (each CHIC has a surface area of 1 cm^2)
t	conduction thickness of the target plate, 0.001143 m
T_n	temperature of n, °C (default T is the fluid temperature)
V	velocity of the fluid in the test section, m/s
w_{mech}	mechanical work, J/kg
z	potential energy term, m

Greek letter symbols

Δp	pressure drop across the HFHE, psi
γ	specific weight of the coolant fluid, N/m^3
λ_n	constant in the wall temperature curve fit, n=0,1,2,3
μ	absolute viscosity of the coolant fluid, N·s/m^2
ν	kinematic viscosity of the coolant fluid, m^2/s
ϕ_n	constant in the $\dot{Q}_{loss}/\dot{Q}_{applied}$ curve fit, n=1,...,7
ρ	density of the coolant fluid, kg/m^3

θ_n constant in the surface temperature curve fit, n=1,2,3
ξ dummy variable to express the direction of the radial heat flow, cm

Subscripts

c refers to the case housing of the electronics
f refers to the coolant fluid
j refers to the junction of the case housing and the electronic chip
s refers to the surface of the HFHE
w refers to the outer wall of the CHIC in the HFHE

INTRODUCTION

Modern aircraft have seen an increase in dependence on electronics. Mackowski (1991) performed an industrial survey to determine future requirements for the high flux heat removal in advanced electronics systems. The study focused on the technology requirements for military avionics systems. The results of this survey can be sorted into four broad application categories: commercial digital systems, military data processors, power processors and radar and optical systems. The most challenging thermal problems were found to lie with the power controllers. The power controllers contain steady-state heat fluxes reaching at least 100 to 200 W/cm^2. In addition, pulsed heat loads of short duration, on the order of a second or less, could exceed 400 W/cm^2. The heat dissipation of future high-performance data processors was predicted to be somewhat lower, with steady-state levels reaching perhaps 50 to 100 W/cm^2.

Flynn (1992) made an evaluation of cooling concepts for high power avionics applications. Based on the results of Mackowski (1991), a steady-state chip heat flux of 100 W/cm^2 and a maximum chip junction temperature of 90°C was selected as representative thermal requirements for near-future high power avionics components. Several additional constraints were also imposed on the cooler due to the intended application of cooling fighter aircraft electronics. These constraints included a practical lower limit on coolant supply temperature, the preference for a non-toxic, nonflammable, and nonfreezing coolant, the need to minimize weight and volume, and operation in an accelerating environment. Evaluation factors included aircraft system impact, cooler development status, and qualitative assessments of life cycle cost, reliability, maintainability, and safety. Among the emerging cooling technologies, seven concepts were identified which could meet the cooling requirements. The evaluated cooling concepts were: Compact High Intensity Cooler (CHIC), Curved Channel Flow with Subcooled Boiling, Evaporative Spray Cooler, Heat Pipe, Jet Impingement with Subcooled Boiling, Microchannel Cooler, and Pumped Capillary Evaporator. These seven cooling concepts were investigated in detail and an assessment of their performance was made against the evaluation factors. The Compact High Intensity Cooler (CHIC) concept was selected to meet the demanding thermal requirements foreseen for near-future avionics. The CHIC device was first introduced by Sundstrand in 1983 (Bland et al., 1983). The original CHIC was developed to provide high intensity (50 W/cm^2) cooling with tight requirements for surface isothermality. This liquid single phase cooler combines the thermal efficiency of multiple jet impingement with a large fin area to produce a high effective heat transfer coefficient.

In the development of the multi-CHIC High Flux Heat Exchanger, Flynn et al. (1994) made a comparison of a single jet impingement to multiple jet impingement. Ordinary jet impingement for a single jet can be divided into three zones: the stagnation zone, the turning region and the wall jet region. For jet impingement with multiple jets a fourth region occurs, the jet interaction zone. These four zones can be seen in Fig. 1. The heat transfer rates are high for both of the inner regions. This leads to the conclusion that a multiple number of small jets will be more effective in cooling the same area than a single large jet. Furthermore, the cooling performance can be enhanced by extending the surface areas. Therefore, a greater surface area density per unit volume can be achieved leading to higher fin efficiencies resulting from the shorter conduction path lengths. This is accomplished by using thin lamination plates in close proximity to the heat source being vigorously scrubbed by high heat transfer coolant jets. This maximizing of the surface area and fin effectiveness is in actuality minimizing the thermal resistance. This concept of using multiple jet impingement with the enhancement of multiple plates is the basis for Sundstrand's development of the CHIC.

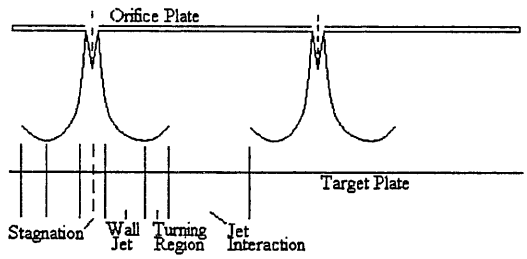

Figure 1. Four characteristic rgions for multiple jet impingement heat exchanger.

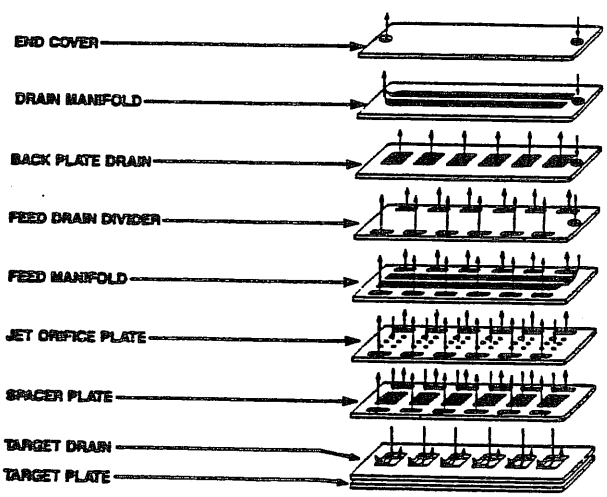

Figure 2. CHIC basic elements and operating principle (Flynn et al., 1994).

The operating principle of a CHIC device is relatively simple, as shown in Fig. 2. The liquid enters the inlet port in the end cover, flows through a succession of thin laminates towards the heat acquisition surface, or target plate. The liquid impinges on the target plate, and then is directed back to the drain manifold attached and ultimately to the exit port of the end cover. The electronics device is attached to the opposite side of the target plate. As shown in Fig. 2, the fluid en route to the target plate passes through a jet orifice plate and a spacer plate. The jet orifice plate usually contains about 50 to 200 small circular holes. In a typical CHIC device, the orifice plate and the spacer plate are repeated several times, with each successive orifice plate acting as a target for the jets from the orifice plate immediately upstream. The orifices are offset by one-half their pitch from plate to plate, so that the liquid impinges on solid metal, then cascades downward as it passes through subsequent orifice plates. The jet interaction of the multiple jets increases the turbulence and mixing, enhancing the heat transfer. Increasing the number of orifice plates, increases the fin area and produces a higher effective heat transfer coefficient. The penalty for a larger number of orifice plates is higher pressure drop and a thicker heat exchanger. Since the 1983 prototype (Bland et al., 1983), several versions of CHICs have been built from copper and aluminum. The devices have been tested with Freon-11 (Bland et al., 1983), Freon-113 (Bland et al., 1990), and water (Grote et al., 1988).

However, this concept only satisfies the requirement for higher heat fluxes caused by modern electronics. To meet the need for an increase in the number of electronic processors, McDonnell Douglas developed the High Flux Heat Exchanger, HFHE. The HFHE consists of 20 CHICs arranged in parallel flow, with each CHIC being 1 cm^2 and capable of absorbing 100 W/cm^2. The HFHE was designed to integrate into the Lockhart LOC-E-JECT liquid cooled Navy Standard Electronic Module (SEM-E) used for F-2 avionics cooling. The actual design requirement for the HFHE is the size must fit the SEM-E, approximately 15 by 17 cm, on 1.5 cm pitch, for a total of 200 cm^2 mounting area per side. Furthermore, the module must absorb 2180 W of steady-state heat load, distributed as 100 W/cm^2 to 20 cm^2 of board surface area, consisting of the 20 one cm^2 CHICs, and 1.0 W/cm^2 heat flux over the remaining 180 cm^2 of surface area. Further details of the high flux heat exchanger design are documented in Flynn et al. (1994).

To ease the process of manufacturing this complex array of CHICs, Sundstrand has developed a process (Flynn and Mackowski, 1993) of photo-etching laminae allowing for very accurate location of the orifices on the plates. The laminae are then stacked and bonded. Diffusion bonding was used for the copper boards and vacuum brazing was used for the aluminum boards. This photo-etching process allows virtually anything that can be drawn to be fabricated.

Because of this need for liquid cooling to absorb higher heat fluxes, additional considerations must be introduced. With the added intermediate aircraft cooling loop associated with liquid cooling, leaking and handling create a selection process for the liquid coolants. And with the increase of emphasis on safety and environmental, this liquid coolant must be non-toxic, non-corrosive, and be an adequate dielectric. In the past, silicate-ester based fluids, Coolanol 25R, were widely used as the liquid coolant in military avionics systems. These fluids have caused significant and sometimes catastrophic problems due to their hygroscopic nature and subsequent formation of flammable alcohols and silica gel. The alcohol by-product lowers the fluid flashpoint, increasing the risk of aircraft fires. The gelatinous precipitate called the "black plague", deposits on the surfaces of the electronics components, causing avionics equipment to malfunction. In order to solve the problems associated with Coolanol, the Air Force and the Navy investigated the possibility of direct replacement of silicate-ester based fluids with hydrogenated polyalphaolefin based fluids. Their studies concluded that polyalphaolefin (PAO) fluids are chemically more stable, (do not hydrolyze to form either silica gel or alcohol by-products), less costly, offer equal or improved dielectric characteristics, and meet or exceed military requirements for a dielectric coolant Gschwender et al. (1985) and Zoppoth and Dillard (1988). Due to these desirable properties of PAO, the Air Force and the Navy, for some selected fighter aircraft, have both replaced the liquid coolant, Coolanol, used in their fighter aircraft electronic cooling systems with PAO.

In a recent study by Ghajar (1993), the hydraulic and thermal performance of PAO and Coolanol 25R in different flow regimes, laminar and turbulent, were compared. The results indicated that at normal operating temperatures the two coolants were reasonably close and fairly independent of the flow regime. However, at low temperatures, dependent on the flow regime, there could be substantial difference between the hydraulic and thermal performance of the two fluids. Particularly, at temperatures below 0°C, PAO's hydraulic performance in the laminar flow region, and its thermal performance in the turbulent flow region, are inferior to those of Coolanol 25R at comparable conditions.

Coolanol has been a standard coolant of fighter aircraft, but is currently being phased out by PAO, which is much less prone to decomposition. Therefore, in this study of the performance for the High Flux Heat Exchanger, PAO was selected as the liquid coolant.

The specific objectives of this research are to investigate the influence of the coolant flow rate and temperature on the pressure drop across the inlet and outlet of the HFHE, to investigate the influence of the coolant flow rate and temperature on the heat flux removal capabilities of the HFHE for steady state heat loads, and to develop a guideline for the performance of the HFHE. This will consist of a performance chart with the necessary coolant flow rate with respect to the coolant temperature to achieve the 100 Watts of heat flux removal and the corresponding charts for the pressure drop for the performance flow rate and temperature.

EXPERIMENTAL SETUP

Both the hydraulic and thermal tests were completed using the test setup as shown in Fig. 3. The liquid coolant, PAO, is pumped from the reservoir, which contains two liters of PAO, to

the in-loop heat exchanger. The pump consists of a constant volume gear pump powered by a Scott Motors variable speed DC motor and connected by a magnetic coupling. The pump-motor is capable of producing flow rates from 30 to over 255 kg/hr. The in-loop heat exchanger consists of a shell and tube heat exchanger with the purpose of keeping the temperature of the PAO constant. This in-loop heat exchanger was necessary due to the use of an outside cold temperature bath. This constant temperature bath consisted of an FTS Systems RC-50 recirculating cooler with FTS Systems HT-30 as the heat transfer fluid. The RC-50 had both a cooling mode and a heating mode, allowing control of the coolant temperature well beyond the temperature range for these tests.

The next component in the test loop is the flow meter. The flow meter consisted of a Micromotion DS25 mass flow meter that had an output of 4 to 24 mA. This output correlated to a flow rate of 0 to 4.32 kg/min. The flow meter was calibrated using the bucket and stopwatch technique, with the output being a linear calibration, ($\dot{m}$ = 0.2406 * mA - 0.9635), with an uncertainty of ± 0.10 kg/min.

After the flow meter, the fluid passes through a 20-micron filter. This filter, made by HYCON, was used to remove particulates that could clog the small coolant passages in the HFHE. Two analog pressure gauges were placed on the inlet and outlet of the filter to monitor the pressure drop across the filter. A high pressure drop reading from the gauges would indicate that the filter needed to be replaced. After any particulates in the fluid have been removed, the coolant enters the test section (HFHE). One quarter inch pressure taps were made immediately upstream of the inlet of the HFHE and immediately downstream of the outlet. The pressure taps were connected to a Validyne P305D-50 wet-wet differential pressure transducer with 0.635 cm vinyl tubing. The differential pressure transducer was calibrated over the range of 0-125 psi (0-862 kPa). Because of the large pressure range, the calibration process itself consisted of a combination of two techniques. For the lower range, 0-50 psi, the transducer was calibrated using a 60-0-60 inch U-tube mercury manometer. For the upper range 50-125 psi, the transducer was calibrated using a dead weight tester. The combination of these two techniques produced a linear curve (Δp = 14.3627 * Voltage - 6.7044) with a corresponding uncertainty of ± 0.05 psi.

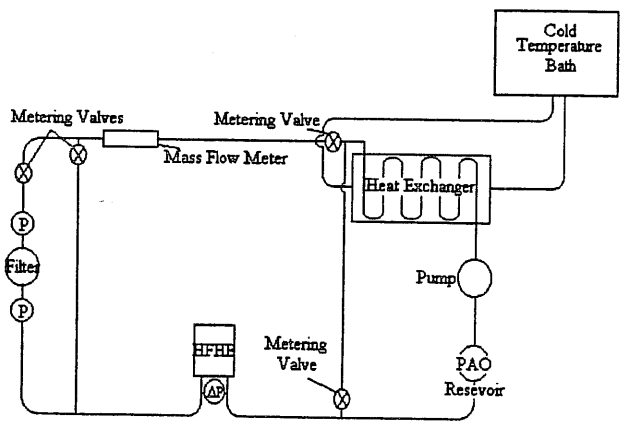

Figure 3. Schematic diagram of the experimental setup.

The last data generating components of the test loop are the thermocouples. The thermocouples consisted of 30-gauge Omega T-type thermocouples and two 1/8 inch Cole Parmer T-type temperature probes. The thermocouples were calibrated over the range of -20 to 60°C, with the use of the constant temperature bath to generate the temperature range and an OMEGA platinum-80 temperature sensor. With this technique, calibration curves were developed for each thermocouple. These calibration curves consisted of a linear curve (thermocouple 15: T_{act}= 1.0009 * T_{meas} - 0.6048) with a typical corresponding uncertainty of ± 0.1°C. The temperature probes were placed at the same location as the pressure taps to give the inlet coolant temperature and the outlet coolant temperature of the HFHE. Furthermore, the individual thermocouples were placed on the surface of the HFHE to generate temperature curves used to develop the equations for the radial heat loss due to conduction from the surrounding CHIC (discussed in the Thermal Performance section). The placement of these thermocouples is shown in Fig. 4.

Also shown in Fig. 4 are the grooves made in the target plate of the HFHE. These grooves allowed for the placement of a thermocouple capable of measuring the wall temperature of the HFHE under operating conditions. These grooves consisted of a channel cut of 0.05 cm in depth across the middle of the target plate for each CHIC. Each component was connected by 1.27 cm I.D. stainless steel tubing and Swedgelock compression fittings.

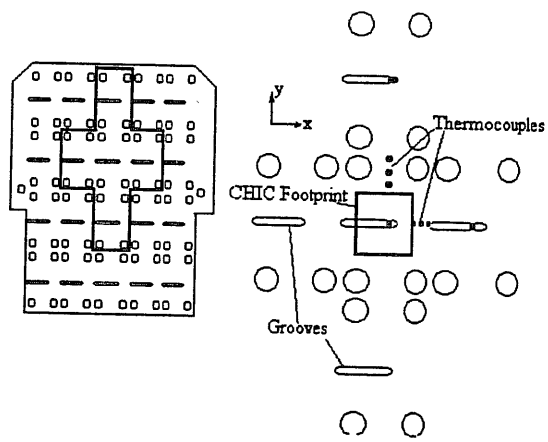

Figure 4. Placement of the surface thermocouples.

The heat source for the thermal tests provided some difficulty because of the high heat fluxes, 100W/cm^2, necessary. Very few dependable heaters are capable of this high heat flux. Therefore, a heat flux amplifier, similar to the one used by Grote et al. (1988), was added to the test setup. The details of this particular heat flux amplifier, given by McDonnell Douglas via Wright Laboratories, are documented in Flynn et al. (1994). Simply, this copper amplifier reduces the heat conduction area from 40.3 cm^2 where the heaters are mounted, to 1.0 cm^2 where the heat is transferred to the HFHE. Thus, low heat flux heating

elements (2.5 W/cm^2) at the top of the amplifier can produce a high heat flux (100 W/cm^2) at the amplifier/HFHE interface. The actual heat source consisted of a Minco mica circular heater with a radius of 2 inches and a resistance of 19 ohms. This heat source is capable of producing heat fluxes, that in conjunction with the amplifier, exceed the 100 W/cm^2 guideline. The lower 1.3 cm of the amplifier has a constant area of one cm^2. In this section, there are three parallel planes of thermocouples spaced 0.25 cm apart. Nine T-type thermocouples are placed at each of the three planes. The temperature at the amplifier/HFHE interface can be approximated by projecting the temperatures in the three planes of the amplifier by using a linear least squares fit. This approximation is used to indicate if the thermocouple placed in the groove is accurate. The thermocouples in the amplifier were calibrated using the same technique as the surface thermocouples and the temperature probes.

The thermocouples, differential pressure transducer, flow meter, and the heater inputs were monitored by a Fluke data processor. The Fluke will contain all of the calibration curves with the output being a DOS data file. A custom data reduction program was then used to generate the final reduced data.

HYDRAULIC PERFORMANCE

The hydraulic tests consisted of pressure drop measurements across the HFHE for ranges of flow rate and inlet coolant temperature of 60 to 240 kg/hr by 15 kg/hr increments and -10 °C to 50 °C by increments of 10 °C, respectively. In addition, because of the emphasis on low temperature measurements for system start up the -15 °C was also included. The actual pressure taps are immediately before and after the inlet and outlet, respectively, of the HFHE. Therefore, the pressure drop measured is the actual pressure drop. The results of these tests are in the form of a family of curves of pressure drops across the range of flow rates and coolant temperatures and the curves corresponding correlation as a function of flow rate and viscosity and as a function of flow rate and coolant temperature. Figure 5 shows the family of curves for the hydraulic performance of the High Flux Heat Exchanger. The next step in the analysis of the hydraulic performance for the HFHE is to determine the equation governing the pressure drop. This is done by the following procedure.

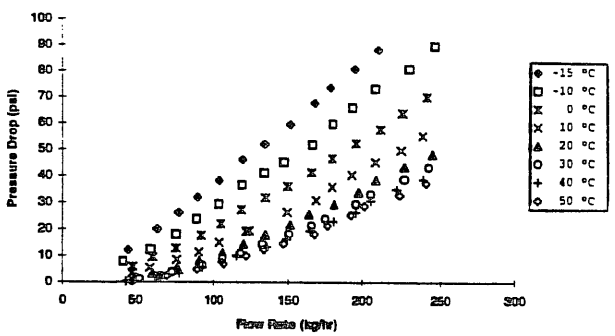

Figure 5. Pressure drop measurements.

First, the steady state incompressible flow energy equation for a control volume in a pipe with several inlet and exit stations can be expressed as follows:

$$w_{mech} = \sum_e \left(\frac{p}{\gamma} + \frac{V^2}{2g} + z\right)_e - \sum_i \left(\frac{p}{\gamma} + \frac{V^2}{2g} + z\right)_i + h_f \qquad (1)$$

However, if the entire HFHE is considered the control volume, only one inlet and one exit station occurs. Also, the friction head loss, h_f, can be expressed by a viscous-frictional loss term and a dynamic loss term. Therefore, the energy equation can be expressed in its final form.

$$\left(\frac{p}{g} + z + \frac{V^2}{2g}\right)_1 + ({}_1w_2)_{mech} = \left(\frac{p}{g} + z + \frac{V^2}{2g}\right)_2 + f\frac{L}{D}\frac{V^2}{2g} + \sum k_i \frac{V^2}{2g} \qquad (2)$$

Now applying this form of the energy equation to the HFHE in the test loop, the following modifications can be made. First, the HFHE is located in the horizontal plane, therefore the change of potential energy across the HFHE, z_1-z_2, can be neglected. In addition, because the hydraulic tests were performed for an isothermal condition, the density of the PAO can be considered a constant across the HFHE. Applying a constant density with the fact that the cross-sectional area of the inlet equals the cross-sectional area of the outlet translates to the velocity entering the HFHE being equal to the velocity exiting the HFHE. Therefore, the change in kinetic energy, $(V^2/2)_1$-$(V^2/2)_2$, across the control volume can also be neglected. Finally, each the viscous-friction term and the dynamic term can be modeled by a summation of the individual viscous-friction terms and dynamic terms associated with the individual plates in each CHIC. Therefore, the equivalent tube-orifice model can be expressed as:

$$\Delta p = \sum_{i=1}^{n} k_i \frac{V_i^2 \rho}{2g_c} + \sum_{i=1}^{n} f_i \frac{L_i}{D_i} \frac{\rho V_i^2}{2g_c} \qquad (3)$$

Now assuming that the flow is predominately laminar flow, the friction factor can be expressed as a function of only the Reynolds number. A check on this assumption yields that the maximum Reynolds number, occurring at the extreme temperature of 50°C, flow rate of 240 kg/hr, and pipe diameter of 1.27 cm (inlet and outlet of the HFHE), is 2176. The Reynolds number occurring at the extreme temperature of -10°C, flow rate of 60 kg/hr, and pipe diameter of 1.27 cm is 50. Therefore, the Reynolds number over the entire flow rate range, 60 to 240 kg/hr, and coolant temperature range, -10°C to 40°C, is laminar. Furthermore, although the individual tubes in the HFHE are much smaller than the inlet/outlet pipe, the flow rate through each CHIC is only 1/20 the flow rate through the inlet/outlet pipe. Some turbulence does occur through the abrupt turning of the flow through the CHICs, however, the increased pressure drop due to this turbulence is modeled in the dynamic pressure loss term. Therefore, the assumption that the flow is predominately laminar is valid and the friction factor is expressed as:

$$f = \frac{C}{Re} = \frac{C\mu}{\rho V D} \tag{4}$$

Substituting Eq. (4) and the expression that the velocity is equal to the volumetric flow rate divided by the cross-sectional area, V=Q/A, yields the following equation for the pressure drop across the HFHE:

$$\Delta p = \sum_{i=1}^{n} \rho Q^2 \left(\frac{k_i}{2A_i^2 g_c} \right) + \sum_{i=1}^{n} \mu Q \left(\frac{CL_i}{2g_c A_i D_i^2} \right) \tag{5}$$

Now, the terms in the parentheses, the minor loss coefficient, the cross-sectional area of the individual tubes, the gravitational constant, the length of the individual tubes, the diameter of the individual tubes, and the constant relating the Reynolds number and the friction factor, are independent of the flow rate and the coolant temperature. Therefore, Eq. (5) can be simplified into the following form:

$$\Delta p = C_1 \mu Q + C_2 \rho Q^2 \tag{6}$$

However, the flow rate measured was in terms of the mass flow rate instead of the volumetric flow rate. Therefore, using the expression that the volumetric flow rate is equivalent to the mass flow rate divided by the density of the fluid, the final equation for the pressure drop across the HFHE is:

$$\Delta P = \frac{\left(C_1 \mu \dot{m} + C_2 \dot{m}^2 \right)}{\rho} \tag{7}$$

Because the pressure drops are dependent on the viscosity, density, and flow rate, this set of curves are indicative to the inert properties of the coolant PAO. Therefore, to complete the modeling of the hydraulic performance of the HFHE, equations for the density and the viscosity of the coolant must be developed as functions of the fluid temperature. These equations were developed by Ghajar et al. (1995), and shown below. First, the viscosity of the PAO follows the following equation, in which the viscosity is in m^2/s and the temperature is in K:

$$\nu = \left(10^{\left(\frac{10^{9.67}}{T^{3.923}} \right)} - 0.70 \right) \times 10^{-6} \tag{8}$$

From this equation, it can be seen that the viscosity increases exponentially below 291.7 K or 18.5 °C. The influnce of this exponential increase can be seen in Fig. 5. In addition, the density of the coolant fluid PAO, in kg/m^3, is given as a function of the coolant temperature, in K, by the following equation:

$$\rho = 1.36 \times 10^3 - 4.56T + 0.0157T^2 - 0.280 \times 10^{-4} T^3 + 0.174 \times 10^{-7} T^4 \tag{9}$$

Now substituting Eq. (8) for the viscosity and Eq. (9) for the density into Eq. (7), and realizing that the kinematic viscosity is equal to the absolute viscosity divided by the density, the final equation for the pressure drop (psi) across the HFHE in terms of the mass flow rate (kg/hr), and inlet coolant temperature (K) is obtained:

$$\Delta p = C_1 \left[\left(10^{\left(\frac{10^{9.67}}{T^{3.923}} \right)} - 0.70 \right) \times 10^{-6} \right] \dot{m} + C_2 \frac{\dot{m}^2}{\left(1.36 \times 10^3 - 4.56T + 0.0157T^2 - 0.28 \times 10^{-4} T^3 + 0.174 \times 10^{-7} T^4 \right)} \tag{10}$$

From a curve fit, the constants C_1 and C_2 were determined to be 7354.83 and 0.43, respectively, for all of the inlet coolant temperatures. These constants yield an equation that fits the experimental data at each discrete temperature that has a standard deviation of 1.8 psi and a maximum error of 3.5 psi at a coolant temperature of -15°C and flow rate of 180 kg/hr. This model, as shown in Figs. 6 and 7, fits the data well, especially at medium and high flow rates. The form of the equation of this model is constrained to pass through the origin. This may affect the fit at the low flow conditions. At normal flow, 200 kg/hr, and an inlet temperature of -10°C, the pressure losses are 28% dynamic and 72% viscous-frictional. For the same flow at an inlet temperature of 50°C the losses are 78% dynamic and 22% viscous-frictional. At reduced flow, 100 kg/hr, and an inlet temperature of -10°C, the pressure losses are 16% dynamic and 84% viscous-frictional. For the same flow rate and at an inlet temperature of 50°C the losses are 64% dynamic and 36% viscous-frictional.

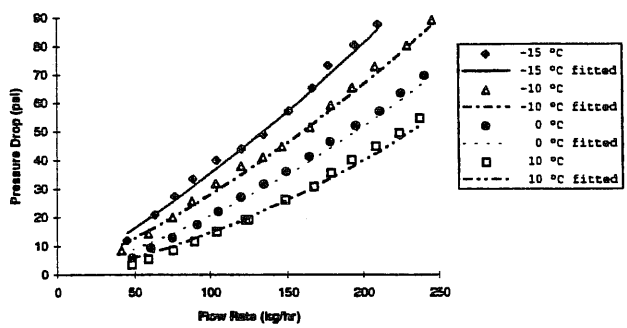

Figure 6. Curve fit for the pressure drop data (-15 to 10°C).

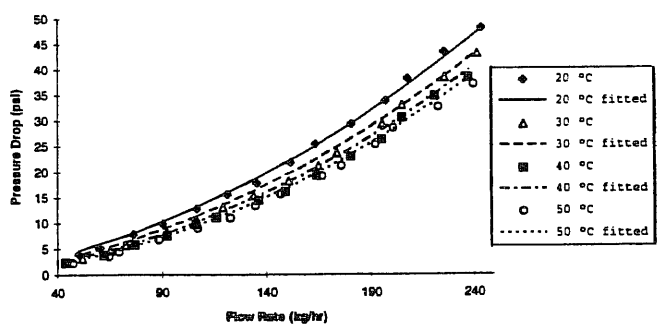

Figure 7. Curve fit for the pressure drop data (20 to 50°C).

THERMAL PERFORMANCE

The thermal tests include the same flow rate range as the hydraulic tests, but the range of inlet coolant temperatures was reduced to -10 °C to 40 °C. This reduction is due to the fact that

the cold temperature bath used to keep the temperature of PAO constant, must actually cool the PAO below -10 °C to remove the power that is added in the thermal tests. In addition, heat loads were applied to the HFHE ranging from 20 W to 100 W by an increment of 20 W. Because the HFHE consists of twenty parallel CHICs, an assumption that all CHICs are identically independent is made. Therefore, the thermal tests consisted of applying a heat load to only one of the CHICs in the HFHE at a time. To check the assumption, numerous CHICs were tested to indicate conformity. However, because of the layout of the CHICs in the HFHE, each CHIC is surrounded by channels of PAO. This results in radial heat loss due to conduction heat transfer when only one CHIC is tested at a time. Therefore, the actual heat flux absorbed by the CHIC is less than the heat load applied. So, a two-dimensional heat transfer model was constructed by taking temperature measurements surrounding the testing CHIC, shown in Fig. 4. The temperature was then plotted and an exponential decaying curve was fitted. This curve fit followed the following equation:

$$T_s = \theta_1 + \theta_2 e^{\theta_3 \xi} \tag{11}$$

Where the variable ξ is a dummy variable representing the distance from the edge of the CHIC in the x or y direction. The constants θ are determined by the curve fit and are dependent on the heat load, fluid temperature, flow rate, and CHIC location. The equation is then differentiated and evaluated at the ξ value representing the symmetry line, shown in Fig. 4. From this temperature gradient, the heat conducted across the line of symmetry in the x and y direction can be approximated from the following equations, respectively:

$$\dot{Q}_{+/-x} = \pi k r_x t \frac{dT_s}{dx}$$
$$\dot{Q}_{+/-y} = \pi k r_y t \frac{dT_s}{dy} \tag{12}$$

This process is a double sided heat transfer model. Therefore, the total heat loss in the radial direction due to conduction heat transfer for a CHIC surrounded by four CHICs would be the sum of the total heat loss in the x-direction and the y-direction. However, if the CHIC being tested was surrounded only by two CHICs (the four corner CHICs), the total heat loss would be one half the sum of the total heat loss in the x-direction and the y-direction. In addition, if the CHIC was surrounded by three CHICs (edge CHICs excluding the corner CHICs), then the total heat loss would be the sum of the heat loss in the direction of the two similar CHICs and one half the heat loss in the direction of the third CHIC. Once the location of the CHICs were accounted for in the total heat loss in the radial direction, it was determined that the individual CHICs tested behaved in similar fashion. This validated the identically independent assumption. The next step in the evaluation of the thermal performance was to develop an analytic equation for the radial heat loss due to conduction heat transfer. In theory, the radial heat loss should be a function of the flow rate only. However, if the energy balance is inspected, it can be shown that the direct path through the CHIC is capable of more heat transfer than the radial path. Therefore, as the heat load is increased, a greater percentage must be transferred directly into the CHIC. This generalization can also be made for the fluid temperature. The affect of the fluid temperature is felt more by the direct route than the radial route. Therefore, as the fluid temperature decreases, a greater percentage of the heat transfer will travel directly into the CHIC. Hence, the actual radial heat loss due to conduction is a function of the flow rate, inlet temperature, and the applied heat load. This is validated by the fact that the largest heat loss occurs at an inlet temperature of 40°C, a flow rate of 60 kg/hr, and a heat load of 20 W. The experimental data was fitted with a curve that was expressed as the following:

$$\frac{\dot{Q}_{loss}}{\dot{Q}_{applied}} = \phi_1 + \left(\phi_2 + \phi_3 e^{(\phi_4 T)}\right) e^{\left(\left(\phi_5 + \phi_6 e^{(\phi_7 T)}\right)\dot{m}\right)} \tag{13}$$

The constants ϕ_n are dependent on the applied heat load. For a heat load of 100 W the constants are as follows: ϕ_1 (0.11858), ϕ_2 (0.11897), ϕ_3 (-0.7860), ϕ_4 (-0.011485), ϕ_5 (-0.0046646), ϕ_6 (-0.37727), and ϕ_7 (-0.017087). The curve fit for the 100 W case is shown in Fig. 8. This curve fit produces equations that have a standard deviation of 0.00053 and a maximum error of 0.0015.

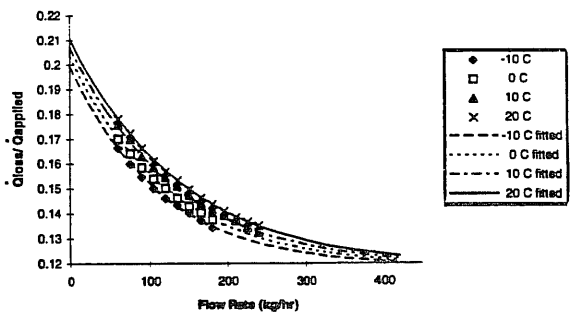

Figure 8. Radial heat loss due to conduction heat transfer for an applied head load of 100 W.

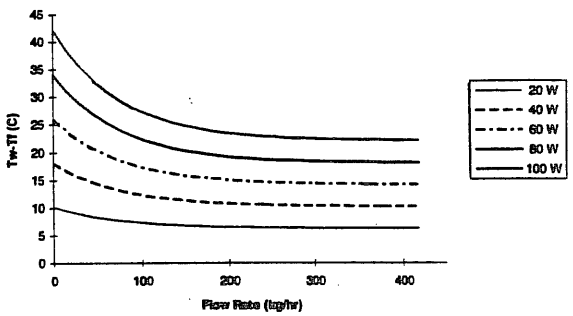

Figure 9. Wall temperature as a function of the flow rate.

The next step in the thermal performance analysis is to develop a thermal resistance equation for the HFHE. To accomplish this, an analytical model must be developed for the wall temperature of the HFHE. This wall temperature theoretically should be a linear function of the heat flux, as shown below:

$$T_w - T_f = \psi \dot{Q} \tag{14}$$

However, the flow rate influences the efficiency of the jet impingement heat exchanger. Therefore, the wall temperature should be a linear function of the heat flux, but the constant, ψ, will be exponentially dependent on the flow rate. To curve fit the experimental data, the heat load used in Eq. (14) must be the net heat load. This is because the wall temperature data was generated by applying a heat load to only one CHIC. However, when a heat load is applied to all twenty CHICs simultaneously, the radial heat loss will be negligible. Thus the net heat load will be approximately the applied heat load. Therefore, the equation for the wall temperature is:

$$T_w - T_f = \lambda_0 + \left(\lambda_1 + \lambda_2 e^{(\lambda_3 \dot{m})}\right)\dot{Q} \tag{15}$$

The constants λ_n are independent of the flow rate, heat load, and fluid temperature and have the following values: λ_0 (2.25), λ_1 (0.19779), λ_2 (0.19968), and λ_3 (-0.013115). This curve fit, shown in Fig. 9, produces a standard deviation of 0.28°C and a maximum error of 0.71°C. Once this equation has been found the thermal resistance of the HFHE can be obtained by the following equation:

$$R_{wf} = \frac{T_w - T_f}{\dot{Q}} \tag{16}$$

This equation can be also expressed in terms of the mass flow rate and the heat load by substituting Eq. (15) into Eq. (16).

$$R_{wf} = \frac{2.25 + \left(0.20 + 0.20e^{(-0.013\dot{m})}\right)\dot{Q}}{\dot{Q}} \tag{17}$$

Once the thermal resistance is calculated, the maximum heat flux capable for the HFHE as a function of the inlet temperature and the flow rate can be calculated using the following equation:

$$\dot{Q} = \frac{T_j - T_f}{R_{jc} + R_{cw} + R_{wf}} \tag{18}$$

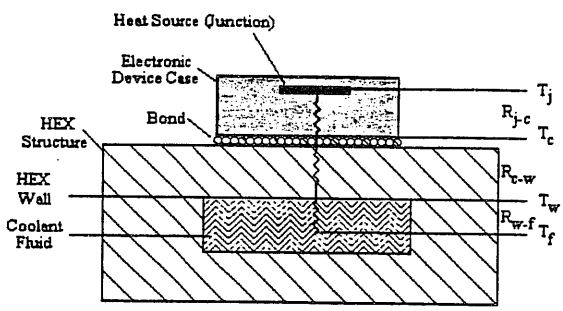

Figure 10. Thermal resistance and junction temperature placement.

The junction temperature was designated by the design requirements of the HFHE to be 90° C. The thermal resistance from the junction to the case interface and the thermal resistance from the case interface to the wall of the HFHE are dependent on the material consistency. The location of these thermal resistances and the junction temperature are shown in Fig. 10. McDonnell Douglas (Flynn et al., 1994) assumed the values of these thermal resistances both to be 0.2°C/(W/cm^2). Therefore, Eq. (18) reduces to a function of the fluid temperature, mass flow rate, and the heat load. Therefore, if Eq. (17) is substituted into Eq. (18), and the resulting equation is solved for the flow rate in terms of the heat load and fluid temperature, the following equation is generated:

$$\dot{m} = -76.24 \ln\left[5.0\left(\frac{-R_{cw}\dot{Q} - R_{jc}\dot{Q} - 2.25 - 0.20\dot{Q} + T_j - T_f}{\dot{Q}}\right)\right] \tag{19}$$

IF $\dot{m}_{measured} \le 0.0$: THEN $\dot{m}_{actual} = 0.0$
ELSE $\dot{m}_{actual} = \dot{m}_{measured}$

A logical expression must be inserted into Eq. (19) because the equation itself does not discern between positive and negative values of the mass flow rate. This logical expression can be added into any control device or computer program and does not invalidate the equation for the mass flow rate. The meaning of this logical expression can be explained as follows. The equation will produce a heat flux capability for the HFHE at zero mass flow rate. The reason for this error is that the equation assumes a constant coolant temperature. However, when zero flow occurs in the HFHE and a heat load is supplied, the coolant temperature increases, thereby invalidating Eq. (19). Therefore, an asymptote must be manually added to the thermal performance curves at zero flow rate. This manual addition is the logical expression. The logical expression itself indicates that any negative values for the flow rate resulting from the input parameters in Eq. (19) in actuality mean that any positive non-zero flow through the HFHE is sufficient to remove the inputted heat flux. Furthermore, a positive value for the mass flow rate resulting from the input parameters in Eq. (19) reflects the actual minimum mass flow rate necessary to remove the given heat flux.

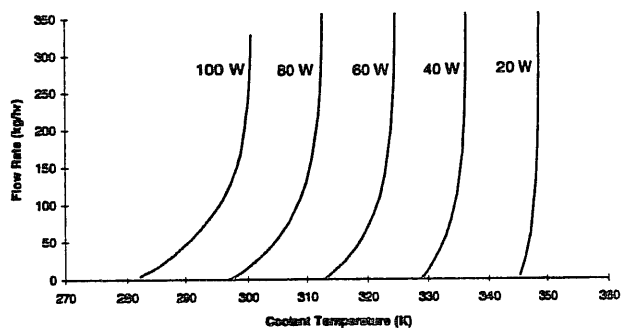

Figure 11. Thermal performance as a function of the heat load junction temperature of 90°C and thermal resistances of 0.20°C/(W/cm^2).

Now if the heat load is held constant, and the values for the thermal resistance and the junction temperatures are assumed to be the values described above, then the flow rate can be

Table 1. Maximum Heat Flux Capability

Pressure Drop		Mass Flow Rate	Junction Temperature	Coolant Temperature	Thermal Resistance (junction to case)	Thermal Resistance (case to wall)	Maximum Heat Flux Capability
kPa	psi	kg/hr	K	K	°C/(W/cm^2)	°C/(W/cm^2)	W/cm^2
311	45	181.68	363	273	0.20	0.20	142.40
311	45	181.68	363	273	0.25	0.25	122.52
311	45	181.68	363	273	0.15	0.15	169.99
311	45	220.47	363	293	0.20	0.20	111.27
311	45	220.47	363	293	0.25	0.25	95.57
311	45	220.47	363	293	0.15	0.15	133.14

calculated as a function of the fluid temperature. These performance curves for a variety of heat loads are shown in Fig. 11. Because the HFHE was designed to remove 100 W per CHIC, an analysis for this applied heat load was performed. As seen in Fig. 11, the flow rate necessary to generate a maximum cooling rate of 100 W per CHIC remains small until the inlet temperature approaches a value of 28°C. At this temperature the minimum flow rate necessary for a cooling rate of 100 W per CHIC increases to infinity. This was reflected in the experimental data. For the value of 0.2 °C/(W/cm^2) for thethermal resistances, R_{jc} and R_{cw}, and a junction temperature of 90°C, the corresponding wall temperature of the HFHE must be 50°C. During experimentation, at coolant temperatures of 30°C and above, the wall temperature exceeded 50°C over the entire range of flow rates. The maximum possible coolant temperature can be increased from 28°C by decreasing the thermal resistances of R_{jc} and R_{cw}. If the thermal resistances were reduced from 0.2 to 0.15 °C/(W/cm^2), the corresponding maximum possible coolant temperature is increased from 28°C to 38°C.

MAXIMUM HEAT FLUX CAPABILITY

The heat flux capability of the HFHE may be estimated by extrapolating the results from Eq. (10) to limit operating conditions specified by the Air Force. These operating conditions include a coolant temperature of 0°C and a pressure drop across the HFHE of 45 psi (311 kPa). Therefore, solving Eq. (10) for the mass flow rate and substituting the operating condition values for the coolant temperature and the pressure drop across the HFHE yields a mass flow rate of 182 kg/hr. Using this value in the HFHE thermal resistance equation, Eq. (17), the thermal resistance can then be solved as a function of the heat flux. This equation can then be substituted into Eq. (18), and solved for the heat flux, shown as Eq. (20).

$$\dot{Q} = \frac{T_j - T_f - 2.25}{R_{cw} + R_{jc} + 0.20 + 0.20e^{(-0.013\dot{m})}} \qquad (20)$$

The operating conditions for the HFHE are as follows: a junction temperature, T_j, of 363 K (90°C), a coolant temperature, T_f, of 273 K (0°C), thermal resistances, R_{cw} and R_{jc}, of 0.20 °C/(W/cm^2), and a mass flow rate, $\dot{m}$, of 182 kg/hr. With these inputs, the maximum heat flux capability of the HFHE is calculated to be 142.4 W/cm^2. However, this maximum heat flux capability is not an absolute. The maximum heat flux is dependent on the operating coolant temperature and thermal resistances between the case and the junction and between the case and the wall. Therefore, the variation in the heat flux capability for the HFHE is shown in Table 1. As a note, for each new coolant temperature, the mass flow rate must be recalculated for the total pressure drop to remain constant at 45 psi (311 kPa). As can be seen, although a higher mass flow rate is capable at the higher coolant temperatures, the coolant temperature remains as the driving factor in the heat flux As can be seen from Table 1, if the refrigeration cycle for the avionic electronic system is capable of coolant temperature below 293 K (20°C) or if the thermal resistance between the junction and the wall of the HFHE can be maintained below 0.2 °C/(W/cm^2), then the HFHE's cooling capacity is well above the required 100 W/cm^2.

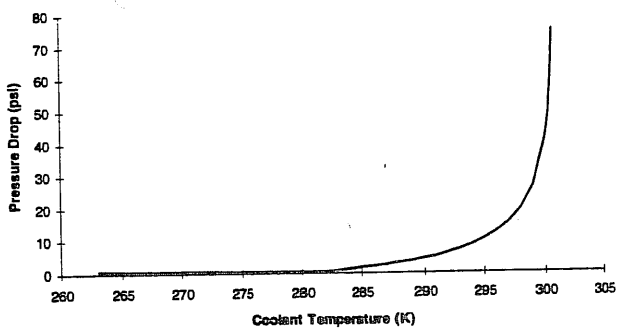

Figure 12. Dynamic hydraulic performance curve for the minimum cooling rate of 100 W per CHIC (T_j = 90°C, R_{jc} = R_{cw} = 0.2°C/(W/cm^2)).

CONCLUSIONS

As seen in Fig. 11, the inlet temperature is critical for the performance of the HFHE. If the coolant temperature is kept below 20°C, then the corresponding minimum flow rate for a cooling rate of 100 W per CHIC can be kept under 70 kg/hr. To further show the importance of the coolant temperature on the performance of the HFHE, Eq. (19), with $\dot{Q}$ = 100 W per CHIC, T_j = 90°C; $R_{jc} = R_{cw}$ = 0.2°C/(W/cm^2), was substituted into Eq. (10), the pressure drop as a function of the flow rate and the coolant temperature. The result is an equation for the pressure drop as a function of the coolant temperature for an applied heat load of 100 W per CHIC. This result is shown in Fig. 12, and, as expressed earlier, if the coolant temperature can be kept below 20°C, then the minimum pressure drop across the HFHE needed for a cooling rate of 100 W per CHIC is 7.2 psi (50 kPa). However, the pressure drop in this equation is the dynamic pressure drop only. As expressed in the hydraulic section of this paper, as the fluid temperature decreases below 18°C, the viscosity of the fluid begins to increase exponentially. Therefore, as the coolant temperature reaches extremely low temperatures, < 0°C, the viscosity is large enough to create a substantial difference in the friction coefficient. Therefore, the pressure drop needed to initiate the flow through the HFHE will be substantially larger than the dynamic pressure drop across the HFHE when the coolant temperature is below 0°C. Hence, it is critical that the inlet temperature remain between 0°C and 20°C. In a practical sense, this can be accomplished by placing a temperature sensor in the actual electronic coolant loop. This sensor should trigger a secondary refrigeration unit to maintain the coolant temperature between 0°C and 20°C. In addition, a control device should be included into the electronic coolant loop to control the flow rate as the coolant temperature varies. Finally, if the above conditions are met, a pump for the electronic coolant loop can be sized by the performance curve pressure and the pressure drop through the rest of the coolant loop.

ACKNOWLEDGEMENT

This research was conducted under sponsorship of the Air Force Wright Laboratory, Aero Propulsion and Power Directorate, Wright Patterson AFB, Ohio, with Dr. Jerry E. Beam and Dr. John E. Leland as Project Managers.

REFERENCES

Mackowski, M. J., 1991, "Requirements for High Flux Cooling of Future Avionics Systems," SAE Paper No. 912104.

Flynn, E. M., 1992, "Evaluation of Cooling Concepts for High Power Avionics Applications," SAE Paper No. 921942.

Bland, T. J., Niggemann, R. E., and Parekh, M. B., 1983, "A Compact High Intensity Cooler (CHIC)," SAE Paper No. 831127.

Flynn, E. M., Downing, R. S., and Nguyen, D. C., 1994, "High Flux Heat Exchanger," Wright Laboratory Final Report No. WL-TR-94-2043, Wright Patterson AFB, OH.

Bland, T. J., Ciaccio, M. P., Downing, R. S., and Smith, W.G., 1990, "The Development of Advanced Cooling Methods for High-Power Electronics," SAE Paper No. 901962.

Grote, M. G., Hendron, R. E., Kipp, H. W., and Lapinski, J. R., 1988, "Test Results of Wafer Thin Coolers at Heat Fluxes from 5 to 125 W/cm^2," SAE Paper No. 880997.

Flynn, E. M., and Mackowski, M. J., 1993, "High Flux Heat Exchanger," Wright Laboratory Interim Report No. WL-TR-93-2027, Wright Patterson AFB, OH.

Gschwender, L. J., Snyder, C. E., and Conte, A. A., 1985, "Polyalphaolefins as Candidate Replacements for Silicate Ester Dielectric Coolants in Military Applications," Lubrication Engineering Journal, Vol. 41, No. 4, pp. 221-228.

Zoppoth, R. C., and Dillard, J., 1988, "PAO Report: Extended Testing of Polyalphaolefins as a Dielectric/Coolant Fluid," Texas Instruments, Defense Systems and Electronics Group, Dallas, Tx.

Ghajar, A. J., 1993, "Comparison of Hydraulic and Thermal Performances of PAO and Coolanol 25R Liquid Coolants," Final Report, Summer Faculty Research Program, Wright Laboratory, Wright Patterson AFB, OH.

Ghajar, A. J., Tang, W. C., and Beam, J. E., 1995, "Methodology for Comparison of Hydraulic and Thermal Performance of Alternative Heat Transfer Fluids in Complex Systems," Heat Transfer Engineering, Vol. 16, No. 1, pp. 68-72.